Mineralogical Magazine (2024), **88**, 546–556
doi:10.1180/mgm.2024.31

CAMBRIDGE UNIVERSITY PRESS

Article

Comparative study on ionic dissolution and structural changes of montmorillonite, kaolinite and muscovite during interfacial reactions with oxalic acid solution

Nanominerals and mineral nanoparticles – thematic issue

Li Zeng, Tongjiang Peng, Hongjuan Sun, Xiyue Zhang and Dingran Zhao

Education Ministry Key Laboratory of Solid Waste Treatment and Resource Recycle, Southwest University of Science and Technology, Mianyang 621010, China

Abstract

Organic acids are commonly found in soils and sediments, playing an important role in the alteration and weathering of minerals and influencing a series of geochemical processes such as soil fertility, metal cycling and pollutant migration. In order to better comprehend the reaction mechanisms of different layered silicate minerals with organic acids, three minerals with various structure types, namely montmorillonite, kaolinite and muscovite, were investigated in this work. In particular, the effects of interfacial reactions with oxalic acid on the crystal structure, chemical composition, morphology and specific surface area of minerals were compared. The composition and structure of montmorillonite, kaolinite and muscovite during the interfacial reaction with oxalic acid were characterised using powder X-ray diffraction (XRD), scanning electron microscopy (SEM) and inductively coupled plasma-optical emission spectroscopy (ICP-OES) methods. It was shown that Si^{4+} and Al^{3+} were dissolved gradually during the interfacial reactions and that the changes in the properties of minerals depended on structural characteristics. After 300 days of the interfacial reactions with oxalic acid, the dissolution percentages of Si^{4+} and Al^{3+} in montmorillonite, kaolinite and muscovite were 12.7%, 8.4%, 3.8% and 62.1%, 30.7%, 6.1%, respectively. Moreover, the lamellar morphology of montmorillonite was destroyed upon the interfacial reaction with oxalic acid, and irregular particles with sizes of ~100–500 nm were formed on the surface. The diameter of kaolinite flake particles decreased from 400–1500 nm to 50–400 nm, and the surface of rod-shaped particles was ruptured. The small particles disappeared from the muscovite surface, and the initially sharp edges became blunted. The specific surface area and the total pore volume of montmorillonite and kaolinite increased after the interfacial reaction with oxalic acid, whereas the opposite results were obtained for muscovite. The differential dissolution of the minerals during their interfacial reaction with oxalic acid was mainly related to the differences between cation occupancies, structural types, chemical bond strengths and specific surface areas.

Keywords: montmorillonite; kaolinite; muscovite; oxalic acid; ionic dissolution; structural evolution

(Received 27 December 2023; accepted 15 April 2024; Accepted Manuscript published online: 5 June 2024)

Introduction

Low-molecular-mass organic acids are widespread in the rhizosphere soil, taking their origin from the decomposition of plants and animal remains, plant root secretions and microbial synthesis (Chen *et al.*, 2023; Yuan *et al.*, 2023). Being involved in various rhizosphere processes, these organic acids influence soil nutrient release and metal ion complexation/chelation (Liu *et al.*, 2017; Onireti *et al.*, 2017; Xue *et al.*, 2018). Organic acids play an important role in the geochemical processes involved in the weathering and evolution of minerals (Huang and Kiang, 1972; Schliemann and Churakov, 2021a). Both free protons and anionic ligands produced by the hydrolysis of organic acids can promote mineral weathering (Cama and Ganor, 2006). Protons lead to a decrease in the pH of the fluid surrounding the mineral and shift the balance toward dissolution (Furrer and Stumm, 1986), whereas anionic ligands impact the saturation state of the minerals and the coordination morphology of Al^{3+} in the solution (Drever and Stillings, 1997; Kong *et al.*, 2014).

Numerous experimental studies on the dissolution of minerals by organic acids have been reported to date. The protonation of hydroxyl groups on the surface of minerals and the formation of coordination compounds between surface cations and organic ligands weakens the *M*–O bond energy, thus promoting dissolution (Stumm *et al.*, 1985). When organic acid molecules are adsorbed onto the olivine surface, the cations on the surface of olivine are more inclined to bond with oxygen in the carbonyl group (C=O) of the organic acid molecule and the H–O bond in the carboxyl group (COOH) is broken, leading to

Corresponding author: Hongjuan Sun; Email: sunhongjuan@swust.edu.cn
Associate Editor: Runliang Zhu
This paper is part of a thematic set on Nanominerals and mineral nanoparticles
Cite this article: Zeng L., Peng T., Sun H., Zhang X. and Zhao D. (2024) Comparative study on ionic dissolution and structural changes of montmorillonite, kaolinite and muscovite during interfacial reactions with oxalic acid solution. *Mineralogical Magazine* **88**, 546–556. https://doi.org/10.1180/mgm.2024.31

© The Author(s), 2024. Published by Cambridge University Press on behalf of The Mineralogical Society of the United Kingdom and Ireland

hydroxylation of the mineral surface. In this case, the increase in the number of carboxyl groups favours the dissolution process (Sun *et al.*, 2023). It has been pointed out that oxalic acid can increase the dissolution rate of montmorillonite, and the relevant dissolution reaction proceeds through a ligand-promoted mechanism (Ramos *et al.*, 2011). Various experiments on the dissolution of biotite in nitric acid and oxalic acid have shown that ligands exert a smaller impact on the overall dissolution rate compared to the proton-promoted reaction (Cappelli *et al.*, 2020). In particular, the dissolution rate of Si^{4+} in kaolinite is higher in citric acid than that in oxalic acid, whereas the dissolution rate of Al^{3+} in oxalic acid will exceed that in citric acid. Moreover, the synergistic effect of oxalic and citric acid accelerates the dissolution of kaolinite, thereby reducing crystallinity and median diameter and enlarging the specific surface area (Lin *et al.*, 2020). Previous studies have mainly focused on the impacts of different acidic solutions on the same mineral and the changes in structure and properties of the products. However, a comparative analysis of similarities and differences in the interaction mechanism and the evolution of the products of the acidic solution in minerals with different structural types has rarely been carried out to date.

Herein, the composition and structural changes of montmorillonite, kaolinite and muscovite during the interfacial reactions with the oxalic acid solution were compared on the basis of their particular polymorphic characteristics. The Si^{4+} and Al^{3+} ions released upon the interfacial reaction between minerals with different layers and structures and acid water were determined. In addition, the similarities and differences in dissolution rates of SiO_4 tetrahedron and AlO_6 octahedron were established. The mechanisms by which the interfacial reactions with acids would affect the crystal structure, chemical composition, morphology and specific surface area of montmorillonite, kaolinite and muscovite were also revealed. The findings of this work provide a basis for investigating the transformations in the composition and structure of minerals under weathering conditions.

Experiment

Materials

Montmorillonite (Mnt) was collected in Yanting country, Sichuan province, China; muscovite (Ms) was obtained in Lingshou country, Hebei province, China; and kaolinite (Kln) came from Suzhou city, Jiangsu province, China. The minerals were prewashed with deionised water under continuous stirring for 24 h after grinding, filtered and dried in an oven at 60°C, and then ground through a 200-mesh sieve. The chemical compositions of montmorillonite, kaolinite and muscovite are listed in Table 1 and the relevant chemical formulae are presented in Table 2.

The chemical formulas of montmorillonite, kaolinite and muscovite are calculated using the following method. By measuring the mass fraction in the chemical composition of the mineral sample, the number of individual atoms was calculated according to the principle of balance between the total amount of negative charges and the total amount of positive charges (i.e. in tetrahedral and octahedral sheets and the interlayer domains) in the general formula of the mineral structure, and then allocated to the tetrahedral, octahedral and interlayer domain locations (if any).

Experimental (considering montmorillonite as an example)

First, 1 g of montmorillonite was put into a 250 mL conical flask, and 100 mL of 0.1 mol·L^{-1} oxalic acid and 1 mL of 0.001 mol·L^{-1} sodium azide (NaN_3) were then added to inhibit microbial growth. The flask was shaken to ensure the full contact between montmorillonite and the organic acids. The flask was afterwards placed in incubator at 25°C and stirred for 2 min every day. After a certain reaction period (30, 60, 90, 120, 150, 180, 210, 240, 270 and 300 days), the conical flask was removed from the incubator, and the supernatant and filter residue were collected. Then, 5 mL of the reactant supernatant was taken and filtered through a 0.45 μm microporous filter for further analysis. The remaining reactants in the flask were filtered to separate the solids from the liquids and rinsed with deionised water until the pH level of 7 was achieved. The filtrate residue was dried at 60°C in an oven for 8 h and then ground and prepared for use. The reactions of muscovite and kaolinite with oxalic acid were conducted conforming to the above steps. The samples after the reaction of montmorillonite, kaolinite and muscovite with oxalic acid solution were named Mnt-t, Kln-t and Ms-t, where t denotes reaction time (day).

Characterisation

The phase composition of the samples was studied via X-ray diffraction (XRD, Ultima IV, Rigaku, Japan) with Cu*K*α radiation (λ = 1.5406 nm) over a 2θ angular range of 3–50° at the step size of 0.02° and the scan rate of 2 s/step in continuous scanning mode using an X'celerator detector. The full elemental chemical

Table 1. Chemical composition of montmorillonite, kaolinite and muscovite.

Samples	SiO_2	Al_2O_3	Fe_2O_3	K_2O	MgO	CaO	Na_2O	TiO_2	Others	LOI	Total
Montmorillonite	56.53	18.31	2.48	0.60	5.26	2.74	0.14	0.18	0.21	13.55	100.00
Kaolinite	43.31	35.55	0.90	0.86	0.18	0.12	0.06	0.19	2.08	16.75	100.00
Muscovite	50.45	30.04	4.37	8.61	0.55	0.21	0.67	0.73	0.23	4.14	100.00

Table 2. Chemical formula of montmorillonite, kaolinite and muscovite.

Samples	Chemical formula
Montmorillonite	$(Ca_{0.20}Mg_{0.06}K_{0.05}Na_{0.02})(H_2O)_n\{(Al_{1.38}Mg_{0.48}Fe_{0.13}Ti_{0.01})[(Si_{3.89}Al_{0.11})O_{10}(OH)_2]\}$
Kaolinite	$(Al_{1.94}Fe_{0.03}Ti_{0.01}Mg_{0.01})[Si_2O_5](OH)_4$
Muscovite	$(K_{0.87}Na_{0.10}Ca_{0.02})\{(Al_{1.67}Fe_{0.25}Mg_{0.05}Ti_{0.04})[Al_{1.11}Si_{2.89}O_{10}](OH)_2\}$

https://doi.org/10.1180/mgm.2024.31 Published online by Cambridge University Press

composition of the samples was analysed by X-ray fluorescence (XRF) spectroscopy (ARL Perform`X, Thermo Fisher, USA) by melting at 1050°C using $Li_2B_4O_7$ as the melting agent. The element detection limit was 100 mg·L^{-1}. The dissolution concentrations of Si^{4+} and Al^{3+} were analysed by inductively coupled plasma-optical emission spectroscopy (ICP-OES, iCAP6500, Thermo Fisher, USA) with a power of 1150 W, pump speed of 50 rpm, auxiliary gas flow rate of 0.5 L·min^{-1} and nebuliser gas flow rate of 0.55 L·min^{-1}. The detection limits of Si^{4+} and Al^{3+} were 0.02 mg·L^{-1} and 0.009 mg·L^{-1}, respectively. The morphology of each composite was examined by field emission-scanning electron microscopy (SEM, sigma300, Zeiss, Germany) with a working voltage of 5 kV, for which the samples were spread onto aluminium sheets and coated with a thin layer of gold using a sputtering machine. The infrared absorption characteristics of the samples were investigated by Fourier-transform infrared spectroscopy (FTIR, Nicolet-5700, Nicolet, USA). The tablet was pressed after mixing and grinding the sample with KBr powder. Nitrogen adsorption and desorption experiments were conducted with a specific surface area and porosity tester (Autosorb IQ, Anton Paar Quanta, USA) under degassing conditions at 100°C for 7 h and the nitrogen temperature of −196°C. The loss on ignition of mineral samples was measured using a programmed controlled muffle furnace (KSD-6-1300, Jinguan Electromechanical Equipment, China). During the experiments, 1.000 g of sample powder pre-dried at 105°C was burned in a muffle furnace at 950°C for 2 h, and the loss on ignition of the sample was then determined by calculating the weight loss percentage.

Calculation of dissolution amount and dissolution rate

The amount of dissolution $S_{i,t}$ (mmol·g^{-1}) and the rate of dissolution $R_{i,t}$ (mmol·g^{-1}·day^{-1}) of the ion, i, in the mineral after reaction time t are calculated by using equations (1) and (2), respectively:

$$S_{i,t} = \frac{(C_{i,t} - C_{i,t_0}) \cdot V}{m_0 \cdot M_i} \quad (1)$$

$$R_{i,t} = \frac{S_{i,t}}{t - t_0} \quad (2)$$

where $C_{i,t}$ and C_{i,t_0} are the dissolved concentration (measured by ICP-OES) of ion i at reaction time t and t_0, respectively, (in mg·L^{-1}); V is the volume of the reaction solution (in L); m_0 is the initial mineral mass (in g); M_i is the molar mass of ion i, (in g·mol^{-1}); and t is the reaction time (in days).

Results and discussion

Phase and structural characteristics

The XRD patterns of the original montmorillonite, kaolinite and muscovite are shown in Fig. 1 together with the products obtained after the interfacial reaction with oxalic acid. The main mineral phase of the montmorillonite was Ca-montmorillonite, with small amounts of illite and quartz (Mnt, Fig. 1a). With the increase in the reaction time between the montmorillonite and the oxalic acid, the (001) peak of montmorillonite has gradually broadened and shifted towards the lower angles. The d values, the intensity ratios of the strongest diffraction peaks to the (101) peak of quartz, and full width at half maximum (FWHM) values of montmorillonite, kaolinite and muscovite are listed in Table 3, together with those of the products obtained after the reaction with oxalic acid. After the reaction with oxalic acid for 150 and 300 days, the 2θ value of the FWHM of the montmorillonite (001) peaks increased from 0.839° to 2.021° and 2.413°, respectively, and the corresponding d_{001} value increased from 15.5864 Å to 16.1793 Å and 16.6069 Å, respectively. The increase

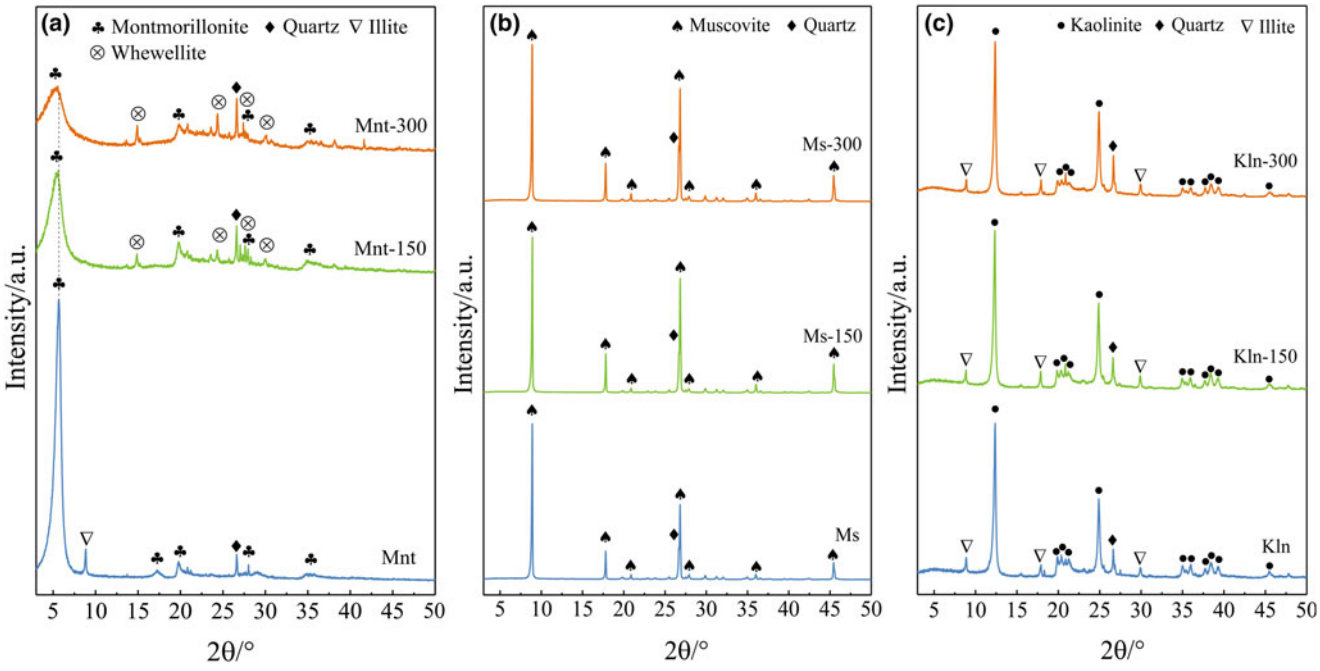


Figure 1. XRD patterns of montmorillonite (a), kaolinite (b), and muscovite (c) after 150 and 300 days of the interfacial reactions with oxalic acid. The dashed line in (a) shows the 001 peak shifting with increased days of reactions.

https://doi.org/10.1180/mgm.2024.31 Published online by Cambridge University Press

Table 3. The *d* values, peak strength, and FWHM of montmorillonite, kaolinite and muscovite after reaction with oxalic acid.

Samples	Characteristics	Reaction time (days)		
		0	150	300
Montmorillonite	d_{Mnt001} (Å)	15.5864	16.1793	16.6069
	I_{Mnt001}/I_{Qz101}	10.398	2.041	1.129
	FWHM (°)	0.839	2.021	2.413
Kaolinite	d_{Kln001} (Å)	7.1514	7.1683	7.1458
	I_{Kln001}/I_{Qz101}	5.242	4.748	3.450
	FWHM (°)	0.295	0.289	0.248
Muscovite	d_{Ms002} (Å)	9.9260	9.9293	9.9229
	I_{Ms002}/I_{Qz101}	4.858	3.857	2.793
	FWHM (°)	0.108	0.113	0.123

in the d_{001} value and FWHM of montmorillonite was due to the replacement of the smaller interlayer $[Ca(H_2O)_6]^{2+}$ (effective diameter = 600 pm) and $[Mg(H_2O)_6]^{2+}$ (effective diameter = 800 pm) ions in the interlayer domain with $[H(H_2O)_n]^+$ (effective diameter = 900 pm) from the solution, which augmented the interlayer spacing in montmorillonite (Kielland, 1937; Wang *et al.*, 2024). In addition, calcium oxalate appeared in the physical phase, which was due to the dissolution of Ca^{2+} in the interlayer and their combination with oxalic acid. The main mineral phase of the kaolinite sample was kaolinite, containing a small amount of illite and quartz (Fig. 1b) and the main mineral phase in the muscovite sample was muscovite, with small amounts of quartz (Fig. 1c). With the increase in interfacial reaction time with oxalic acid, the change in the d_{001} value of kaolinite, d_{002} value of muscovite and FWHMs of both minerals were minimal, indicating that their crystallinity degree remained high. According to Table 3, the ratios of the strongest peaks of montmorillonite, kaolinite and muscovite to the (101) peaks of quartz decreased gradually, among which the I_{Mnt001}/I_{Qz101} ratio demonstrated the most pronounced decrease. This indicates that oxalic acid has affected montmorillonite, kaolinite and muscovite to a greater extent than quartz. Moreover, the results indicated that the crystal structure of montmorillonite underwent the maximum changes, which was related to the structure of the expandable crystal layer of montmorillonite (Robin *et al.*, 2017), where H^+ was more likely to enter into the interlayer and exchange with the cations during the reaction (Laszlo, 1987). As a result, H^+ was more likely to attack hydroxyl in the structure, promoting the dissolution of montmorillonite and breakdown of its structure.

Ionic dissolution

The variation curves of the dissolution amounts of Si^{4+} and Al^{3+} with time during the reactions of montmorillonite, kaolinite and muscovite with oxalic acid are shown in Fig. 2, which demonstrates that the reactions of the minerals with oxalic acid led to the dissolution of the cations in their structure, among which the dissolved amounts of Si^{4+} and Al^{3+} of kaolinite and muscovite increased gradually with the lengthening of the reaction time, whereas the dissolved amount of Si^{4+} in montmorillonite showed an alternate tendency. This was attributed to the formation of acid insoluble amorphous silica upon the reaction, which interfered with the measured Si^{4+} concentration. After the interfacial reaction with oxalic acid, montmorillonite exhibited a higher solubility of Si^{4+} and similar solubility of Al^{3+} relative to kaolinite, whereas muscovite had lower solubility of Si^{4+} and Al^{3+}. As the reaction of montmorillonite with oxalic acid induced the formation of amorphous silica, thereby affecting the dissolution process of Si^{4+}, the amount of Si^{4+} and Al^{3+} dissolved in oxalic acid in the total content of the mineral, that is, the dissolution percentage, was further calculated, and the results are shown in Table 4. After 300 days of the reaction with oxalic acid, the dissolution percentages of Si^{4+} and Al^{3+} in montmorillonite, kaolinite and muscovite were 12.7%, 8.4%, 3.8% and 62.1%, 30.7%, 6.1%, respectively. It was evident that oxalic acid had a greater influence on the dissolution of cations in montmorillonite, followed by kaolinite and muscovite. The variation curves of the dissolution rates of Si^{4+} and Al^{3+} with time during the reactions of montmorillonite, kaolinite and muscovite with oxalic acid are shown in Fig. 3. The figure illustrates that at the initial stage of the reaction, all three minerals underwent fast dissolution of Si^{4+} and Al^{3+}, which was attributed to the dissolution of fine particles and the defect sites within the large grains (Kalinowski and Schweda, 1996; Huertas *et al.*, 1999). On the first day of the reaction, montmorillonite had the largest dissolution rates of Si^{4+} and Al^{3+}, followed by muscovite and kaolinite. The dissolution rates of Si^{4+} and Al^{3+} in montmorillonite remained the greatest even after

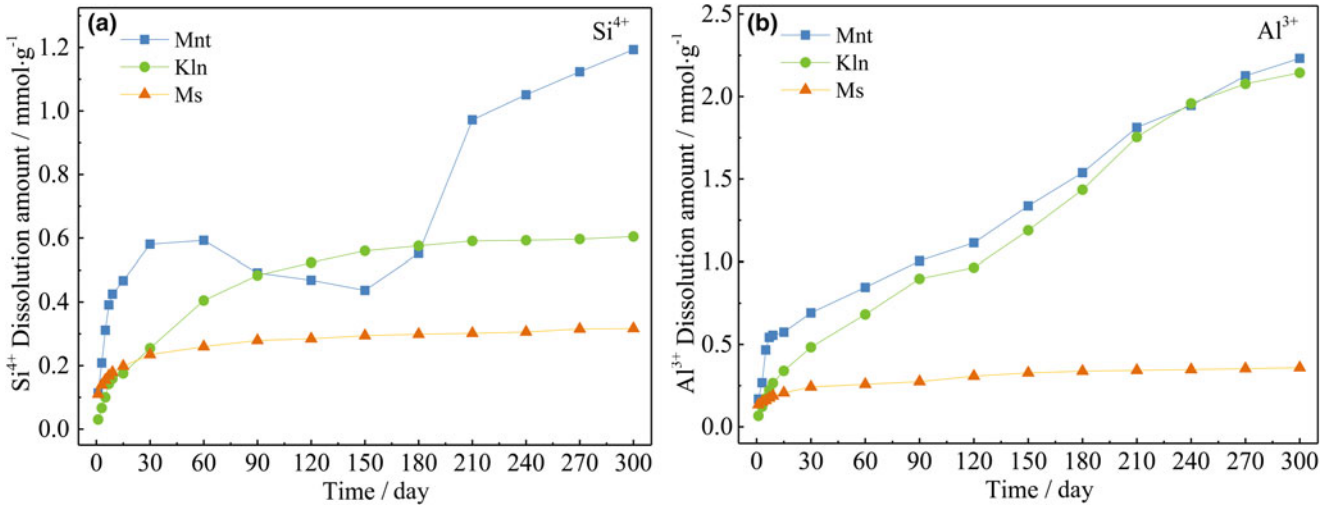


Figure 2. Dissolution amount curves of (a) Si^{4+} and (b) Al^{3+} with time for montmorillonite, kaolinite and muscovite samples with oxalic acid.

https://doi.org/10.1180/mgm.2024.31 Published online by Cambridge University Press

Table 4. Dissolution percentages of Si^4 and Al^{3+} in montmorillonite, kaolinite, and muscovite after reactions with oxalic acid (%).

Samples	Montmorillonite			Kaolinite			Muscovite		
Duration (days)	60	150	300	60	150	300	60	150	300
Si^{4+}	6.3	4.6	12.7	5.6	7.8	8.4	3.1	2.4	3.8
Al^{3+}	23.5	37.2	62.1	9.8	17.0	30.7	3.4	5.6	6.1

3 days of the reaction, while the lower dissolution rates in muscovite were observed consistently over the remaining 297 days. With the progress of the reaction, montmorillonite and kaolinite exhibited similar dissolution rates of Al^{3+}, being an order of magnitude higher than those in muscovite.

The changes in ion dissolution rates in the minerals after the interfacial reactions with oxalic acid were related to a variety of factors, such as particle size, specific surface area and properties of tetrahedral and octahedral cations. Montmorillonite, kaolinite and muscovite belong to dioctahedral phyllosilicate minerals whose basic units are SiO_4 tetrahedral and AlO_6 octahedral sheets. According to the different combinations of basic units, the above minerals can be divided into 1:1 (tetrahedral–octahedral) and 2:1 (tetrahedral–octahedral–tetrahedral) type phyllosilicate minerals. In particular, montmorillonite has a 2:1 layer structure with exchangeable cations (Ca^{2+}, Na^+ and K^+) in the interlayer. When it reacts with oxalic acid, the interlayer cations are preferentially replaced by H^+ and dissolved, and then Al^{3+} and Si^{4+} are gradually dissolved along the edge structure. In this process, H^+ continuously penetrates the structure from the interlayer, and the expansion characteristic of montmorillonite also enlarges the effective area between montmorillonite and acid, thereby accelerating the dissolution of Al^{3+} and Si^{4+}. In turn, kaolinite has a 1:1 layer structure, wherein the theoretical ion dissolution rate increases after the interfacial reaction with oxalic acid. However, it lacks exchangeable cations in the interlayer, making it difficult for penetration of H^+ therein, and it can only destroy the structural layer from the edge. As a result, the dissolution rates of Al^{3+} and Si^{4+} are lower than those in montmorillonite under the same conditions. Finally, muscovite has a 2:1 layer structure with K^+ in the interlayer, but its specific surface area is an order of magnitude smaller than that of montmorillonite. Moreover, the morphology of the muscovite structure is presented by a large layer, whereby the edge of the surface area is negligible compared to the substrate, which reduces the ion dissolution rate. Therefore, the higher ion dissolution rate of muscovite in the early stage of the reaction could be caused by the fracture of the lamellar structure and the exposure of more active edge sites during the grinding and preparation process.

Morphological changes

Scanning electron microscopy images of montmorillonite, kaolinite and muscovite as well as the products after 150 and 300 days of the reaction with oxalic acid are in Fig. 4. Montmorillonite in Fig. 4a–c shows that it aggregated from a lamellar morphology, exhibiting the obvious curling of thin edges. After the reaction with oxalic acid for 150 days, the lamellar morphology was destroyed, and irregular particles with sizes of ~100–500 nm were formed onto the surface. After 300 days of the reaction, these irregular particles became smaller (~50 nm), making the structure loose and porous. Kaolinite in Fig. 4d–f shows that the initial sample was composed of pseudohexagonal lamellae and rod-like particles with a diameter of ~200 nm. After the reaction with oxalic acid for 150 days, the edges of the lamellae were obviously blunted, the particles with diameters of 400–1500 nm were decomposed into those with sizes of 50–400 nm. The outer surface of the rod-shaped particles ruptured with many fine lamellar particles attached to them. The above phenomenon became more obvious after the reaction for 300 days. The initial morphology of muscovite (Fig. 4g) was lamellae with an average size of ~30 μm with fine particles attached to their surface. After 150 days of the reaction with oxalic acid, the amount of fine particles attached to the surface of muscovite decreased, making its smooth, and the initially sharp lamellar edges became blunted (Fig. 4h). After 300 days of the reaction, obvious etching pits appeared on the surface of muscovite, which might be related to the preferential dissolution of defect sites on the surface of the mineral (Fig. 4i).

Molecular vibration and bond energy change

The FTIR spectra of montmorillonite, kaolinite and muscovite as well as their products after 150 and 300 days of the reaction with oxalic acid are shown in Fig. 5. The peaks at 3435 and 1641 cm^{-1} in the spectrum of montmorillonite (Fig. 5a) were caused by the

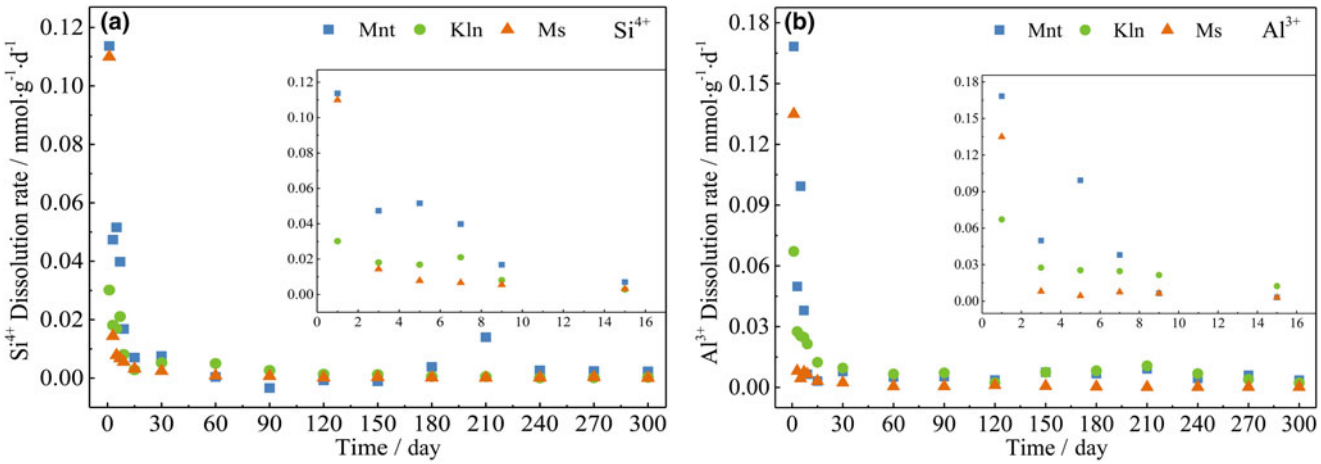


Figure 3. Dissolution rate curves of (a) Si^{4+} and (b) Al^{3+} with time for montmorillonite, kaolinite and muscovite with oxalic acid. The insets show the initial dissolution rates in detail.

https://doi.org/10.1180/mgm.2024.31 Published online by Cambridge University Press

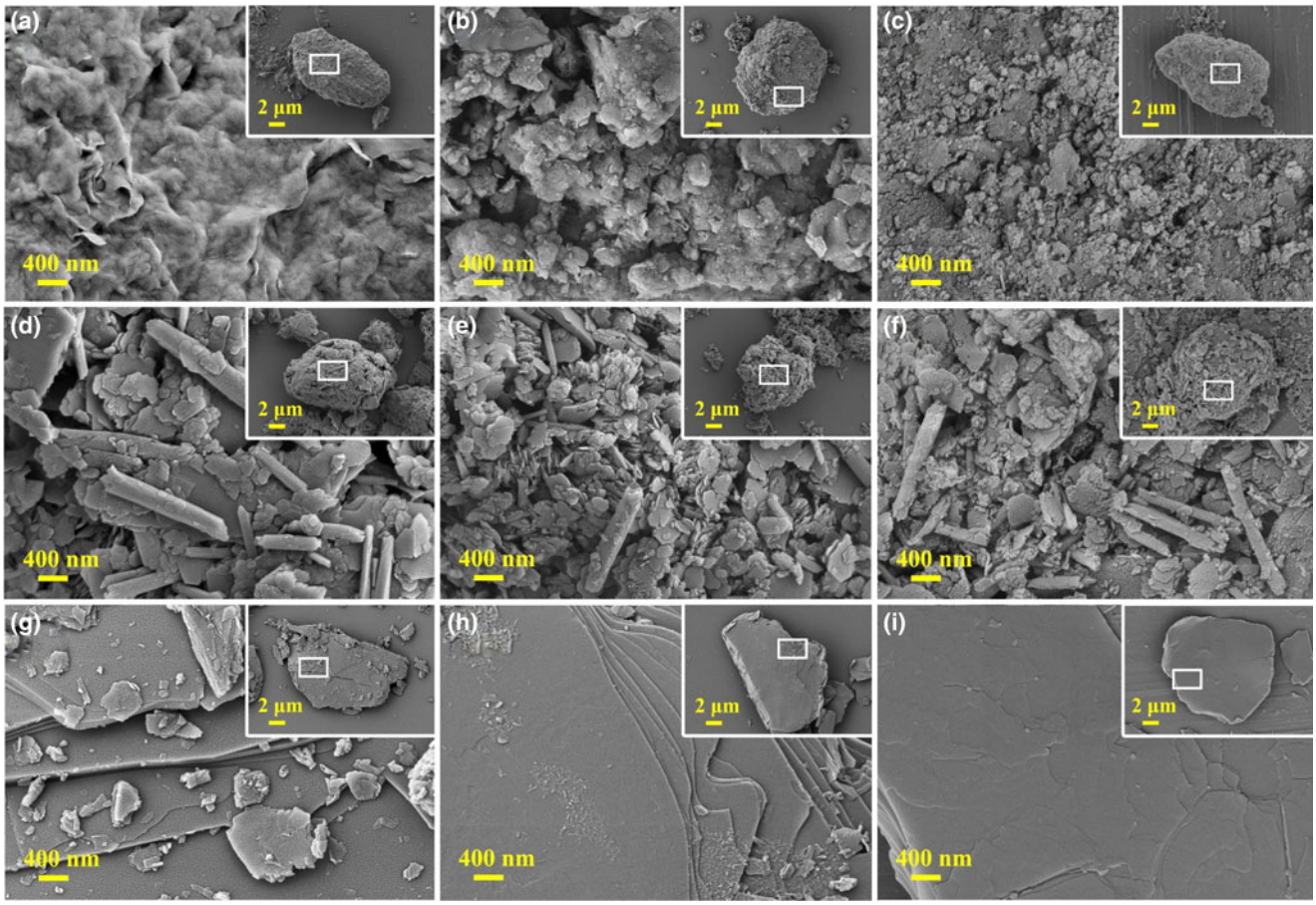


Figure 4. SEM images of montmorillonite, kaolinite and muscovite as well as the products after the reaction with oxalic acid for 150 and 300 days (a) Mnt; (b) Mnt-150; (c) Mnt-300; (d) Kln; (e) Kln-150; (f) Kln-300; (g) Ms; (h) Ms-150; and (i) Ms-300.

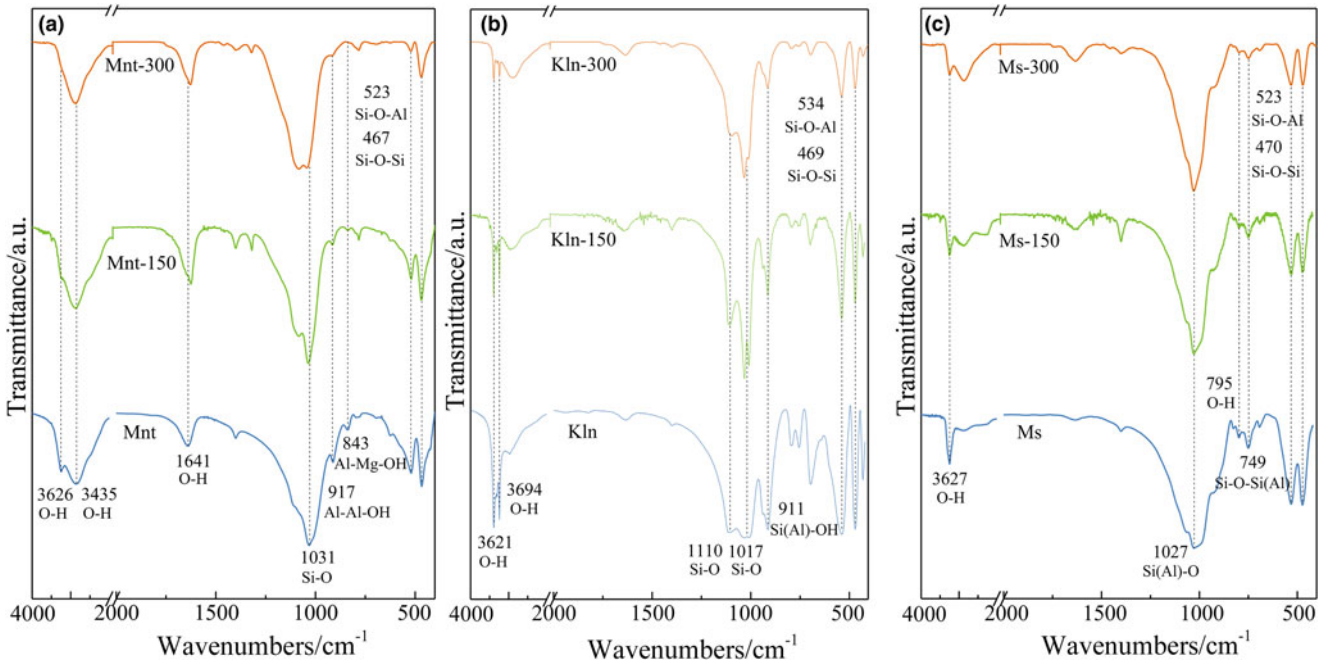


Figure 5. FTIR spectra of (a) montmorillonite, (b) kaolinite and (c) muscovite as well as the products after the reaction with oxalic acid for 150 and 300 days.

https://doi.org/10.1180/mgm.2024.31 Published online by Cambridge University Press

H_2O stretching and bending vibrations in adsorbed and interlayer water in the sample (Deepika and Sethuraman, 2023). Moreover, there was only one O–H stretching vibration peak (at 3626 cm^{-1}) as a result of the combination of hydroxyl group with the Al^{3+} cation (Farmer and Russell, 1964), indicating that the octahedral Al content in the montmorillonite was high. The peaks at 917 cm^{-1} (Al–Al–OH) and 843 cm^{-1} (Al–Mg–OH) confirmed the substitution of octahedral layers (Zhao *et al.*, 2015). The peak at 1031 cm^{-1} was attributed to a Si–O stretching vibration, and the peaks at 523 and 467 cm^{-1} were ascribed to the tetrahedral Si–O–Al and Si–O–Si bending vibrations, respectively (Farmer *et al.*, 1979; Hassanien *et al.*, 2010; Godek *et al.*, 2022). The intensities of the above vibrational peaks gradually decreased after the interfacial reaction with oxalic acid, and the strengths of the Si–O–Al peaks decreased to a greater extent compared with that of Si–O–Si bonding. This result showed that the interfacial reaction with oxalic acid led to the replacement of the ions by protons in the octahedra and tetrahedra of the montmorillonite, and that tetrahedral Si^{4+} were more stable than octahedral Al^{3+}.

According to Fig. 5b, the peak at 3621 cm^{-1} in the spectrum of kaolinite was induced by the O–H stretching vibration of the inner hydroxyl group between tetrahedral and octahedral sheets, and the band at 3694 cm^{-1} was caused by the O–H stretching vibration of the edge hydroxyl group (Farmer and Russell, 1964; Farmer, 1968; Madejová, 2003). The vibrational peaks of the inner and edge hydroxyl groups both decreased with the lengthening of the interfacial reaction with oxalic acid, indicating that protons entered into the structural layer and attacked the hydroxyl groups, leading to dehydroxylation which caused the continuous leaching of Al^{3+} from the octahedral layer (Panda *et al.*, 2010). The peaks at 1110 and 1017 cm^{-1} were assigned to the Si–O stretching vibrations (Wang *et al.*, 2016). With the lengthening of the reaction, the peak at 1017 cm^{-1} was split into the features at 1028 and 1009 cm^{-1}. The peak at 911 cm^{-1} was caused by the Si(Al)–OH bending vibration (Ehsan *et al.*, 2023), and those at 469 and 534 cm^{-1} corresponded to the Si–O–Si and Si–O–Al bending vibrations, respectively, and the intensities of the above-mentioned vibration peaks decreased with the lengthening of the reaction. The changes in the peak intensities at 911, 1009, 1028 and 1110 cm^{-1} indicated that the reaction affected the bonding strength of O–H groups in Si(Al)–O–Al–OH and Si–O in Al(Si)–O–Si–O chains, and the ions at the corresponding positions were replaced by protons (Madejová *et al.*, 1998; Nguetnkam *et al.*, 2011).

Muscovite (Fig. 5c) exhibits the O–H stretching vibrational peak at 3627 cm^{-1}, and the peak at 795 cm^{-1} was attributed to the O–H out-of-plane oscillating absorption (Fan *et al.*, 2023). The peak intensity gradually decreased after the reaction with oxalic acid, indicating that the OH structure was destroyed in the process. The peaks at 1027 and 749 cm^{-1} corresponded to the Si(Al)–O and Si–O–Si(Al) stretching vibrations (Luo *et al.*, 2021), and the features at 523 and 470 cm^{-1} were attributed to the bending vibrations of tetrahedral Si–O–Al and Si–O–Si, respectively. With the lengthening of the reaction, the intensities of the above vibrational peaks decreased gradually. In general, the contents of functional groups in the montmorillonite, kaolinite and muscovite changed by different degrees after the reactions with oxalic acid, which proved the existence of the interaction between H^+ and the mineral structure.

N_2 adsorption–desorption isotherm

The N_2 adsorption–desorption isotherms of montmorillonite, kaolinite and muscovite as well as their products obtained after the reaction with oxalic acid are shown in Fig 6. The isotherms for montmorillonite were similar to the type IV isotherm of the IUPAC classification system, indicating a typical mesoporous structure (Zaghouane-Boudiaf and Boutahala, 2011) with an obvious H3-type hysteresis loop (Vrbková *et al.*, 2023). The isotherms of the kaolinite and muscovite corresponded to those of type-II (Gao *et al.*, 2016), which are generally attributed to nonporous or macroporous materials. The hysteresis loop can reflect the

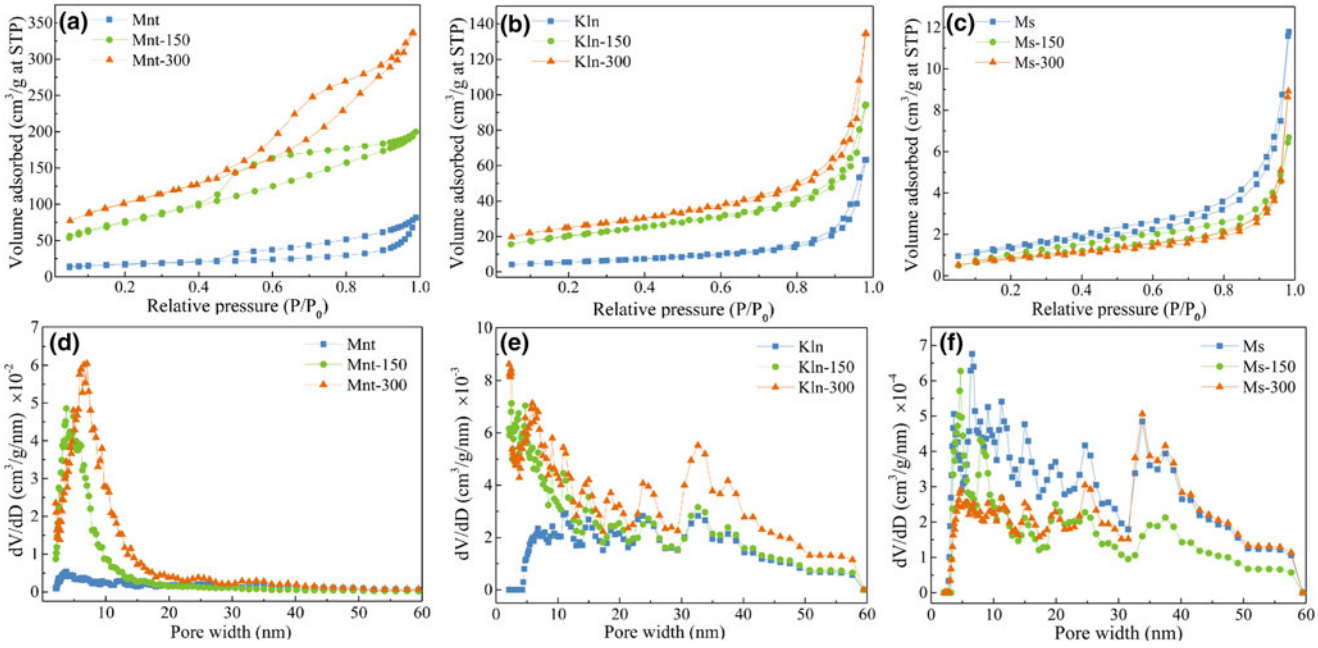


Figure 6. N_2 adsorption–desorption isotherms (a–c) and pore size distribution curves (d–f) of montmorillonite, kaolinite and muscovite as well as the products after the reaction with oxalic acid for 150 and 300 days.

https://doi.org/10.1180/mgm.2024.31 Published online by Cambridge University Press

Table 5. Total pore volume and specific surface area of montmorillonite, kaolinite and muscovite as well as the products after the reaction with oxalic acid.

Samples	Montmorillonite			Kaolinite			Muscovite		
Duration (days)	0 d	150 d	300 d	0 d	150 d	300 d	0 d	150 d	300 d
Specific surface area ($m^2 \cdot g^{-1}$)	58.8	273.3	359.5	19.8	71.2	87.4	5.0	3.3	3.0
Total pore volume ($cm^3 \cdot g^{-1}$)	0.0208	0.0836	0.1198	0.0064	0.0241	0.0306	0.0015	0.0008	0.0008

information about pore distribution and morphology within the specimen (Phadungbut *et al.*, 2016; Toncón-Leal *et al.*, 2021). After the montmorillonite reacted with oxalic acid, the slope of the hysteresis loop increased, indicating the pore morphology changed from slit pores between flaky particles to irregularly internal voids (Sing, 1982). Moreover, no obvious change was observed in the adsorption isotherms of the kaolinite and muscovite after the reaction. The specific surface areas and total pore volumes were calculated on the basis of the obtained adsorption isotherms, the Brunauer–Emmett–Teller method (BET) and Nonlocal-Density-Functional-Theory (NLDFT), and the results are shown in Table 5 and Fig. 6d–f. The pore size distributions of the montmorillonite and kaolinite after the reactions with oxalic acid became wider and the number of pores increased significantly in the range of 2–15 nm. In turn, the pore size distribution in muscovite remained almost unchanged but the porosity decreased significantly. According to Table 5, the specific surface areas of montmorillonite and kaolinite increased by 4.7 and 6.1 times and by 3.6 and 4.4 times after 150 and 300 days of the reaction with oxalic acid, respectively, and the total pore volume also increased to different degrees. The formation of mesopores and micropores occurred due to the partial leaching of Al^{3+} cations from the octahedral sheets (Krupskaya *et al.*, 2019). Furthermore, the dissolution of cations made the particles negatively charged, and the charge repulsions existing between the particles caused the original agglomerates to disintegrate, thus increasing the specific surface area. Although pits and pores were formed during the dissolution of muscovite, the changes were minor compared to those after extensive removal of smaller impurities. The contribution from smaller impurities to the specific surface area was greater than that from pits, resulting in the decrease in the specific surface area and total pore volume of muscovite.

Differential dissolution

A schematic diagram of the reaction process is shown in Fig. 7. During the reactions between minerals and oxalic acid, H^+ ions first enter into the interlayer and exchange with interlayer cations (if any). At the same time, H^+ attacks the Al–O(OH) bonds at the edges of octahedra, allowing Al^{3+} to enter the solution with the hydroxyl groups. In this process, the dissolution of Al^{3+} makes the Si–O tetrahedron at the edge unstable, causing Si^{4+} ions to enter into the solution in the form of H_2SiO_3, which destroys the mineral structure. The differences between the dissolution rates of minerals are related to the variations in particle size, surface charge, mineral structure and specific surface area, which can arise owing to the following reasons. First, compared with the complexity of the interlayer cations in montmorillonite, kaolinite and muscovite exhibit limited homogeneous and heterogeneous ionic substitutions in their crystal lattices, as well as very few cations other than Si^{4+} and Al^{3+}. During the reaction with the acid, the cations in the interlayers in montmorillonite, such as Mg^{2+} and Ca^{2+} are first attacked by H^+, and the continuous penetration of H^+ into the structure accelerates the leaching of Al^{3+}. The leaching of octahedral cations leads to a decrease in crystallinity and the weakening of the interlayer forces, which accelerates the dissolution process. Second, the dissolution rate of the mineral shows a high correlation with the specific surface area. Assuming that the accessibility of N_2 to the minerals is equal to that of oxalic acid, it appears that the specific surface area determined from the N_2 adsorption–desorption isotherm is equal to the contact area between the mineral and oxalic acid. Therefore, the cation dissolution rates of kaolinite and muscovite with relatively small specific surface areas will be much smaller than those of montmorillonite. During the dissolution process, the Al–O(OH) bonds suffer from the impact of oxalic acid only at the edges of the mineral particles, which means that the dissolution starts from the edge hydroxyl groups (Schliemann and Churakov, 2021b), and the size of the edge specific surface area is more important. The morphological analysis indicates that montmorillonite and kaolinite contain more edge structures, whereas the edge surface area in the lamellar structure of muscovite is negligible in relation to that of the basal plane, which reduces its dissolution rate. Third, the specific expandability of montmorillonite not only makes it easy for H^+ to enter into the interlayer and get exchanged with interlayer cations, but also increases the effective interaction area between montmorillonite and the acid, allowing H^+ to attack the tetrahedral Si from the inside and thus accelerating the dissolution. At the same time, the exchanged Ca^{2+} and oxalate ions form calcium oxalate precipitates, which affect the ion balance and eventually cause more serious structural damage.

Conclusion

On the basis of the findings of this study, the main conclusions can be drawn as follows:

(1) The reactions of the minerals with oxalic acid led to the dissolution of ions such as Si^{4+} and Al^{3+}, and the dissolved amount of ions in kaolinite and muscovite increased gradually with the lengthening of the reaction. The reaction of montmorillonite with oxalic acid produced amorphous silica which is insoluble in the acid. The dissolution rate of Al^{3+} was used to assess the effect of oxalic acid on the minerals, which decreased in the following order: montmorillonite, kaolinite and muscovite.
(2) After the interfacial reaction with oxalic acid, the flaky morphology on the surface of montmorillonite was destroyed, and irregular particles with sizes of ~100–500 nm were formed onto the surface. The flake size in kaolinite decreased from 400–1500 nm to 50–400 nm, and the surface of rod-shaped particles was ruptured. The fine particles present on the surface of muscovite disappeared, and the initially sharp lamellar edges became blunted.
(3) The specific surface areas of the products of montmorillonite, kaolinite and muscovite after 300 days of the reactions with

https://doi.org/10.1180/mgm.2024.31 Published online by Cambridge University Press

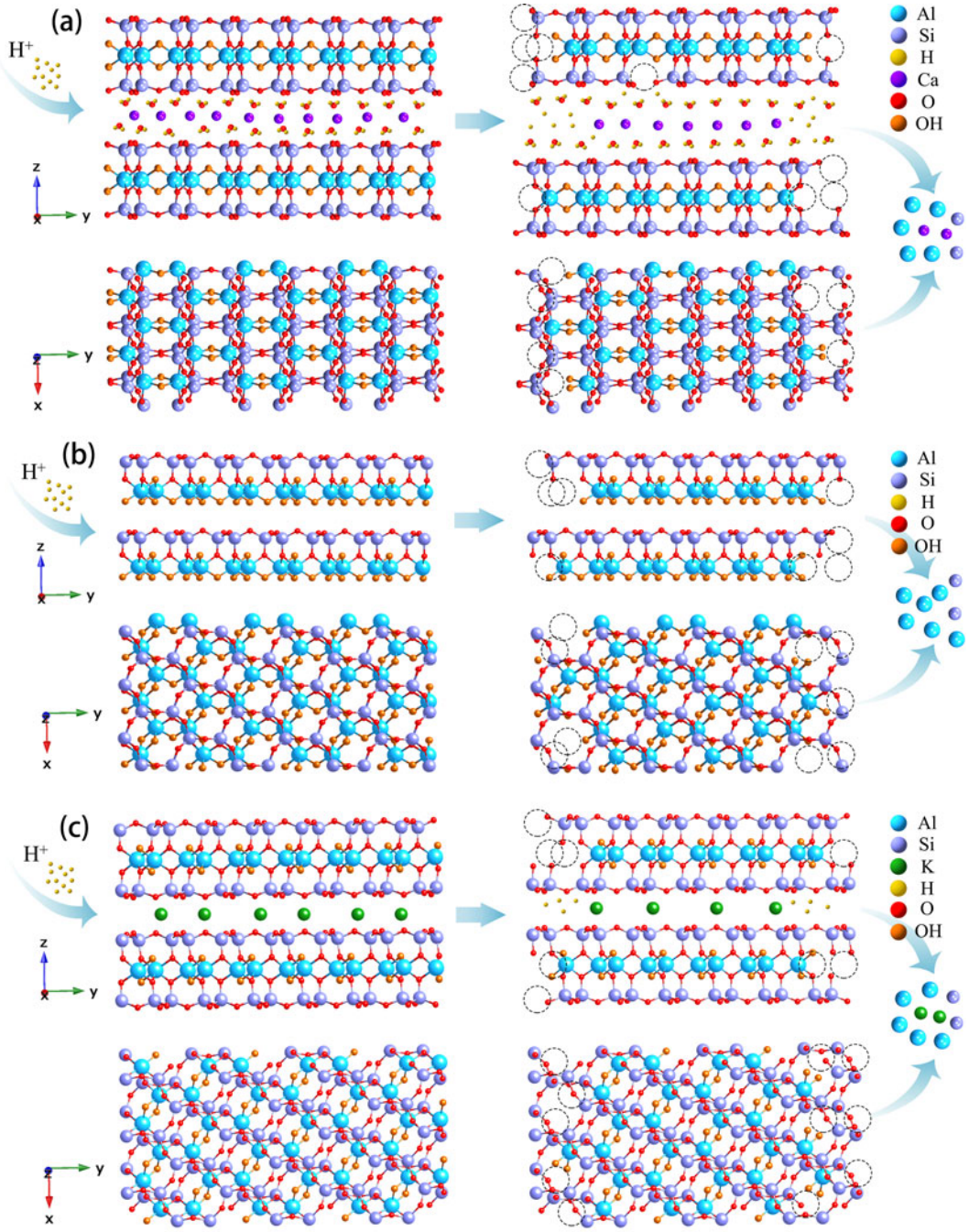


Figure 7. Schematic showing the reaction process between minerals and oxalic acid (a) montmorillonite, (b) kaolinite and (c) muscovite.

oxalic acid were 6.11, 4.41 and 0.60 times that of the original, respectively. In montmorillonite, the slit-like pores between lamellar particles were transformed into irregularly internal voids. The lamellar particles in kaolinite became smaller and the rod particles were ruptured, which led to the increase in the number of mesopores. The reaction between oxalic acid and muscovite enabled removal of surface impurities and exerted a little effect on the morphology.

(4) The differential dissolution of the minerals during the interfacial reaction with oxalic acid was related to the complexity of the interlayer cations, the specific surface area, the number of edge structures and the differences in the properties of the minerals. Compared with kaolinite and muscovite, montmorillonite has abundant interlayer cations and edge structures along with the large interlayer spacing and specific surface area, which are conducive to the increase in ion dissolution rate.

It is worth noting that because this work focuses on the chemical weathering of minerals under acidic conditions, microbial inhibitors (sodium azide, NaN_3) have been added to avoid the influence of microorganisms on the mineral–aqueous interface. In fact, the life activities of microorganisms have a great influence on the dissolution of mineral components. Bacteria and their exometabolites can change the element morphology and saturation state of

https://doi.org/10.1180/mgm.2024.31 Published online by Cambridge University Press

minerals in solutions, and then promote the dissolution of cations in mineral structures (Bundeleva *et al.*, 2014; Lamérand *et al.*, 2020). Fungi affect the weathering of minerals mainly through their selective adhesion to the mineral surface containing growth nutrients, thereby reducing the pH in the environment through the production of organic acids and CO_2 via respiration and thus accelerating the dissolution of minerals (Lamérand *et al.*, 2022; Li *et al.*, 2022). The presence of fungal microorganisms also impacts the mineral formation and transformation, facilitating the conversion of montmorillonite to illite and chlorite to vermiculite (Ross and Kodama, 1976; Biswas *et al.*, 2017). Therefore, the influence of microorganisms on mineral weathering is very complex. Based on the study of the mineral–aqueous interface reactions, the influence of microorganisms can be further explored, which is of significance for in-depth understanding of the mineral weathering in the surface environment.

Declaration of competing interest. The authors declare that they have no known competing financial interests or personal relationships that could have appeared to influence the work reported in this paper.

Acknowledgements. This work was supported by the National Natural Science Foundation of China (grant number 42072048).

References

Biswas B., Chakraborty A., Sarkar B. and Naidu R. (2017) Structural changes in smectite due to interaction with a biosurfactant-producing bacterium Pseudoxanthomonas kaohsiungensis. *Applied Clay Science*, **136**, 51–57.

Bundeleva I.A., Ménez B., Augé T., Bodénan F., Recham N. and Guyot F. (2014) Effect of cyanobacteria Synechococcus PCC 7942 on carbonation kinetics of olivine at 20°C. *Minerals Engineering*, **59**, 2–11.

Cama J. and Ganor J. (2006) The effects of organic acids on the dissolution of silicate minerals: A case study of oxalate catalysis of kaolinite dissolution. *Geochimica et Cosmochimica Acta*, **70**, 2191–2209.

Cappelli C., Cama J., Van Driessche A.E.S. and Huertas F.J. (2020) Biotite reactivity in nitric and oxalic acid at low temperature and acid pH from surface and bulk dissolution measurements. *Chemical Geology*, **554**, 119806–119818.

Chen H., He Z., Hou M., Tang C. and Wu Y. (2023) Adsorption of trichlorphon on phyllosilicate minerals, Effect of low molecular organic acids. *Pedosphere*, **33**, 1–18.

Deepika R. and Sethuraman M.G. (2023) Pd-ZnO nanoparticles decorated acid activated montmorillonite for the efficient removal of cationic dyes from water. *Journal of Molecular Structure*, **1278**, 134910–134924.

Drever J.I. and Stillings L.L. (1997) The role of organic acids in mineral weathering. *Colloids and Surfaces A, Physicochemical and Engineering Aspects*, **120**, 167–181.

Ehsan M.F., Barai H.S., Islam M.M., Susan M.A., Joo S.W. and Miran M.S. (2023) ZnO nanocomposites supported by acid-activated kaolinite as photocatalysts for the enhanced photodegradation of an organic dye. *Materials Today Communications*, **36**, 106563–106575.

Fan C., Ren L., Zhang Y. and Bao S. (2023) Grinding effect of sodium silicate on muscovite and its mechanism analysis. *Minerals Engineering*, **199**, 108106–108114.

Farmer V.C. (1968) Infrared spectroscopy in clay mineral studies. *Clay Minerals*, **7**, 373–387.

Farmer V.C. and Russell J.D. (1964) The infra-red spectra of layer silicates. *Spectrochimica Acta*, **20**, 1149–1173.

Farmer V.C., Fraser A.R. and Tait J.M. (1979) Characterization of the chemical structures of natural and synthetic aluminosilicate gels and sols by infrared spectroscopy. *Geochimica et Cosmochimica Acta*, **43**, 1417–1420.

Furrer G. and Stumm W. (1986) The coordination chemistry of weathering, I. Dissolution kinetics of δ-Al_2O_3 and BeO. *Geochimica et Cosmochimica Acta*, **50**, 1847–1860.

Gao W., Zhao S., Wu H., Deligeer W. and Asuha S. (2016) Direct acid activation of kaolinite and its effects on the adsorption of methylene blue. *Applied Clay Science*, **126**, 98–106.

Godek E., Grządka E. and Maciołek U. (2022) Influence of polysaccharides with different chemical character on stability of montmorillonite suspensions in the presence of pseudoamphoteric cocamidopropyl betaine. *Journal of Molecular Liquids*, **357**, 119097–119110.

Hassanien M.M., Abou-El-Sherbini K.S. and Al-Muaikel N.S. (2010) Immobilization of methylene blue onto bentonite and its application in the extraction of mercury (II) *Journal of Hazardous Materials*. **178**, 94–100.

Huang W.H. and Kiang W.C. (1972) Laboratory dissolution of plagioclase feldspars in water and organic acids at room temperature. *American Mineralogist*, **57**, 1849–1859.

Huertas F.J., Chou L. and Wollast R. (1999) Mechanism of kaolinite dissolution at room temperature and pressure Part II, kinetic study. *Geochimica et Cosmochimica Acta*, **63**, 3261–3275.

Kalinowski B.E. and Schweda P. (1996) Kinetics of muscovite, phlogopite, and biotite dissolution and alteration at pH 1–4, room temperature. *Geochimica et Cosmochimica Acta*, **60**, 367–385.

Kielland J. (1937) Individual activity coefficients of ions in aqueous solutions. *Journal of the American Chemical Society*, **59**, 1675–1678.

Kong M.M., Huang L., Li L.F., Zhang Z.Y., Zheng S.X. and Wang M.K. (2014) Effects of oxalic and citric acids on three clay minerals after incubation. *Applied Clay Science*, **99**, 207–214.

Krupskaya V., Novikova L., Tyupina E., Belousov P., Dorzhieva O., Zakusin S., Kim K., Roessner F., Badetti E., Brunelli A. and Belchinskaya L. (2019) The influence of acid modification on the structure of montmorillonites and surface properties of bentonites. *Applied Clay Science*, **172**, 1–10.

Lamérand C., Shirokova L.S., Bénézeth P., Rols J. and Pokrovsky O.S. (2020) Olivine dissolution and hydrous Mg carbonate and silicate precipitation in the presence of microbial consortium of photo-autotrophic and heterotrophic bacteria. *Geochimica et Cosmochimica Acta*, **268**, 123–141.

Lamérand C., Shirokova L.S., Bénézeth P., Rols J. and Pokrovsky O.S. (2022) Carbon sequestration potential of Mg carbonate and silicate biomineralization in the presence of cyanobacterium Synechococcus. *Chemical Geology*, **599**, 120854.

Laszlo P. (1987) Chemical reactions on clays. *Science*, **235**, 1473–1477.

Li Z., Liu L., Lu X., Cao Y., Ji J. and Chen J. (2022) Hyphal tips actively develop strong adhesion with nutrient-bearing silicate to promote mineral weathering and nutrient acquisition. *Geochimica et Cosmochimica Acta*, **318**, 55–69.

Lin S.M., Yu Y.L., Zhang Z.J., Zhang C.Y., Zhong M.F., Wang L.M., Lu S.X., Xu W., Li N. and Huang X. (2020) The synergistic mechanisms of citric acid and oxalic acid on the rapid dissolution of kaolinite. *Applied Clay Science*, **196**, 105756–105766.

Liu G.C., Chen L., Jiang Z.X., Zheng H., Dai Y.H., Luo X.X. and Wang Z.Y. (2017) Aging impacts of low molecular weight organic acids (LMWOAs) on furfural production residue-derived biochars, Porosity, functional properties, and inorganic minerals. *Science of The Total Environment*, **607–608**, 1428–1436.

Luo D.X., Geng R.Y., Wang W., Ding Z., Qiang S.R., Liang J.J., Li P., Zhang Y.X. and Fan Q.H. (2021) Trichoderma viride involvement in the sorption of Pb(II) on muscovite, biotite and phlogopite, Batch and spectroscopic studies. *Journal of Hazardous Materials*, **401**, 123249–123259.

Madejová J. (2003) FTIR techniques in clay mineral studies. *Vibrational Spectroscopy*, **31**, 1–10.

Madejová J., Bujdák J., Janek M. and Komadel P. (1998) Comparative FT-IR study of structural modifications during acid treatment of dioctahedral smectites and hectorite. *Spectrochimica Acta Part A Molecular & Biomolecular Spectroscopy*, **54**, 1397–1406.

Nguetnkam J.P., Kamga R., Villiéras F., Ekodeck G.E., Razafitianamaharavo A. and Yvon J. (2011) Alteration of cameroonian clays under acid treatment. Comparison with industrial adsorbents. *Applied Clay Science*, **52**, 122–132.

Onireti O.O., Lin C. and Qin J. (2017) Combined effects of low-molecular-weight organic acids on mobilization of arsenic and lead from multi-contaminated soils. *Chemosphere*, **170**, 161–168.

Panda A.K., Mishra B.G., Mishra D.K. and Singh R.K. (2010) Effect of sulphuric acid treatment on the physico-chemical characteristics of kaolin clay. *Colloids and Surfaces A, Physicochemical and Engineering Aspects*, **363**, 98–104.

Phadungbut P., Do D.D. and Nicholson D. (2016) On the microscopic origin of the hysteresis loop in closed end pores – Adsorbate restructuring. *Chemical Engineering Journal*, **285**, 428–438.

https://doi.org/10.1180/mgm.2024.31 Published online by Cambridge University Press

Ramos M.E., Cappelli C., Rozalén M., Fiore S. and Huertas F.J. (2011) Effect of lactate, glycine, and citrate on the kinetics of montmorillonite dissolution. *American Mineralogist*, **96**, 768–780.

Robin V., Tertre E., Beaucaire C., Regnault O. and Descostes M. (2017) Experimental data and assessment of predictive modeling for radium ion-exchange on beidellite, a swelling clay mineral with a tetrahedral charge. *Applied Geochemistry*, **85**, 1–9.

Ross G.J. and Kodama H. (1976) Experimental alteration of a chlorite into a regularly interstratified chlorite-vermiculite by chemical oxidation. *Clays and Clay Minerals*, **24**, 183–190.

Schliemann R. and Churakov S.V. (2021a) Atomic scale mechanism of clay minerals dissolution revealed by ab initio simulations. *Geochimica et Cosmochimica Acta*, **293**, 438–460.

Schliemann R. and Churakov S.V. (2021b) Pyrophyllite dissolution at elevated pressure conditions, An ab initio study. *Geochimica et Cosmochimica Acta*, **307**, 42–55.

Sing K. (1982) Reporting physisorption data for gas/solid systems with special reference to the determination of surface area and porosity. *Pure and Applied Chemistry*, **54**, 2201–2218.

Stumm W., Furrer G., Wieland E. and Zinder B. (1985) The effects of complex-forming ligands on the dissolution of oxides and aluminosilicates. *The Chemistry of Weathering*, **149**, 55–74.

Sun C., Yao Z., Wang Q., Guo L. and Shen X. (2023) Theoretical study on the organic acid promoted dissolution mechanism of forsterite mineral. *Applied Surface Science*, **614**, 156063–156075.

Toncón-Leal C.F., Villarroel-Rocha J., Silva M.T.P., Braga T.P. and Sapag K. (2021) Characterization of mesoporous region by the scanning of the hysteresis loop in adsorption–desorption isotherms. *Adsorption*, **27**, 1109–1122.

Vrbková E., Vaňková M., Lhotka M. and Vyskočilová E. (2023) Acid treated montmorillonite – efficient catalyst in Prins reaction of alpha-methylstyrene with paraldehyde. *Molecular Catalysis*, **542**, 113143–113152.

Wang H., Feng Q. and Liu K. (2016) The dissolution behavior and mechanism of kaolinite in alkali-acid leaching process. *Applied Clay Science*, **132–133**, 273–280.

Wang M., Rivenbark K.J. and Phillips T.D. (2024) Kinetics of glyphosate and aminomethylphosphonic acid sorption onto montmorillonite clays in soil and their translocation to genetically modified corn. *Journal of Environmental Sciences*, **135**, 669–680.

Xue X.P., Xu Z.H., Israel P. and Li P. (2018) Interaction between low molecular weight carboxylic acids and muscovite, Molecular dynamic simulation and experiment study. *Colloids and Surfaces A, Physicochemical and Engineering Aspects*, **559**, 8–17.

Yuan L.M., Wu Y.Q., Fan Q.H., Li P., Liang J.J., Liu Y.H., Ma R., Li R.J. and Shi L.P. (2023) Influence mechanism of organic matter and low-molecular-weight organic acids on the interaction between minerals and PAHs. *Science of the Total Environment*, **862**, 160872–160882.

Zaghouane-Boudiaf H. and Boutahala M. (2011) Kinetic analysis of 2,4,5-trichlorophenol adsorption onto acid-activated montmorillonite from aqueous solution. *International Journal of Mineral Processing*, **100**, 72–78.

Zhao Y.H., Wang Y.J., Hao Q.Q., Liu Z.T. and Liu Z.W. (2015) Effective activation of montmorillonite and its application for Fischer-Tropsch synthesis over ruthenium promoted cobalt. *Fuel Processing Technology*, **136**, 87–95.

https://doi.org/10.1180/mgm.2024.31 Published online by Cambridge University Press